Analysis of fusion-fission dynamics by pre-scission neutron emission in ^{58}Ni+^{208}Pb

Y. Aritomo [a] M. Ohta [b] T. Materna [c] F. Hanappe [c] O. Dorvaux [d] L. Stuttge [d]

[a] *Flerov Laboratory of Nuclear Reactions, JINR, Dubna, Russia*

[b] *Department of Physics, Konan University, 8-9-1 Okamoto, Kobe, Japan*

[c] *Universite Libre de Bruxelles, 1050 Bruxelles, Belgium*

[d] *Institut de Recherches Subatomiques, F-67037 Strasbourg Cedex, France*

Abstract

We analyzed the experimental data of the pre-scission neutron multiplicity in connection with fission fragments in the reaction ^{58}Ni+^{208}Pb at the incident energy corresponding to the excitation energy of compound nucleus E^*=185.9 MeV, which was performed by DéMoN group. The relation between the pre-scission neutron multiplicity and each reaction process having different reaction time is investigated. In order to study the fusion-fission process accompanied by neutron emission, the fluctuation-dissipation model combined with a statistical model is employed. It is found that the fusion-fission process and the quasi-fission process are clearly distinguished in correlation with the pre-scission neutron multiplicity.

Key words: superheavy elements, fluctuation-dissipation dynamics, fusion-fission process, quasi-fission process, pre-scission neutron multiplicity

1 Introduction

Many experiments on the induced fission at near and below Coulomb barrier in superheavy-mass region have been done and the mass and kinetic energy distributions of fission fragments were measured (1). In these phenomena, the reaction process is classified into several characteristic processes, they are the fusion-fission process (FF), the quasi-fission process (QF) and the deep inelastic collision process (DIC). Depending on the shell effect of the compound nucleus or the composite nucleus, the deep quasi-fission process (DQF) can be seen in a certain reaction system (2). In the DQF process, mass symmetric fission fragments are observed but no compound nucleus is formed.

Each process has its own characteristic reaction time from the contact of the colliding partner to the scission point. This was shown by the dynamical calculation for the time development of the nuclear shape in terms of the Langevin equation (2). The different reaction time means that each reaction process associates the different pre-scission neutron multiplicity.

We undertake to extend our model discussed in reference (2), by taking into account the effect of neutron emission. We combine the Langevin calculation with the statistical model which calculates the neutron emission. We apply our model to the recent experiment, in which the pre-scission neutron multiplicity correlated with the mass distribution of fission fragments has been measured in the reaction ^{58}Ni+^{208}Pb at the incident energy corresponding to the excitation energy of compound nucleus $E^* = 185.9$ MeV. This experiment was done by DéMoN group (3). The feature of distribution of pre-scission neutron multiplicity ν_n has two distinct components, one located around $\nu_n = 4$ and the other around $\nu_n = 8$. This structure may be sign of two mechanisms having two different life-time of the composite system, they are, the QF process and the FF process. By our model calculation, it can be clearly shown the two components of the neutron multiplicity are corresponding to the above two processes.

In this paper, we show theoretically the usefulness of the methods of classifying the dynamical process on the basis of the pre-scission neutron multiplicity correlated with the mass distribution of fission fragments. This approach is a powerful tool for investigating fusion-fission mechanism and for estimating precise cross section relevant to the problem on superheavy elements synthesis.

In section 2, we briefly explain our framework for the study and the model. We discuss the pre-scission neutron multiplicity in correlation with fission fragments in section 3. We also present how the pre-scission neutron multiplicity depends on the strength of the friction, the level density parameter and the neutron binding energy used in the statistical model. In section 4, we present a summary and further discussion to clarify the reaction mechanism in superheavy mass region.

2 Model

Using the same procedure as described in reference (2) to investigate the fusion-fission process dynamically, we use the fluctuation-dissipation model and employ the Langevin equation. We adopt the three-dimensional nuclear deformation space given by two-center parameterization (4; 5). The neck parameter ϵ is fixed to be 1.0 in the present calculation, so as to retain the contact-like configuration more realistically for two-nucleus collision. The three

collective parameters involved in the Langevin equation are as follows: z_0 (distance between two potential centers), δ (deformation of fragments) and α (mass asymmetry of the colliding nuclei); $\alpha = (A_1 - A_2)/(A_1 + A_2)$, where A_1 and A_2 denote the mass numbers of the target and the projectile, respectively.

The multidimensional Langevin equation is given as

$$\begin{aligned}
\frac{dq_i}{dt} &= \left(m^{-1}\right)_{ij} p_j, \\
\frac{dp_i}{dt} &= -\frac{\partial V}{dq_i} - \frac{1}{2}\frac{\partial}{\partial q_i}\left(m^{-1}\right)_{jk} p_j p_k - \gamma_{ij}\left(m^{-1}\right)_{jk} p_k + g_{ij} R_j(t),
\end{aligned} \tag{1}$$

where a summation over repeated indices is assumed. q_i denotes the deformation coordinate specified by z_0, δ and α. p_i is the conjugate momentum of q_i. V is the potential energy, and m_{ij} and γ_{ij} are the shape-dependent collective inertia parameter and dissipation tensor, respectively. A hydrodynamical inertia tensor is adopted in the Werner-Wheeler approximation for the velocity field, and the wall-and-window one-body dissipation is adopted for the dissipation tensor (6; 7; 8). The normalized random force $R_i(t)$ is assumed to be white noise, *i.e.*, $\langle R_i(t)\rangle$=0 and $\langle R_i(t_1)R_j(t_2)\rangle = 2\delta_{ij}\delta(t_1 - t_2)$. The strength of random force g_{ij} is given by $\gamma_{ij}T = \sum_k g_{ij}g_{jk}$, where T is the temperature of the compound nucleus calculated from the intrinsic energy of the composite system as $E_{int} = aT^2$, with a denoting the level density parameter. The temperature-dependent potential energy is defined as

$$V(q, l, T) = V_{DM}(q) + \frac{\hbar^2 l(l+1)}{2I(q)} + V_{shell}(q)\Phi(T), \tag{2}$$

$$V_{DM}(q) = E_S(q) + E_C(q), \tag{3}$$

where $I(q)$ is the moment of inertia of a rigid body at deformation q, V_{shell} is the shell correction energy at $T = 0$, and V_{DM} is the potential energy of the finite-range liquid drop model. E_S and E_C denote a generalized surface energy (9) and Coulomb energy, respectively. The centrifugal energy arising from the angular momentum l of the rigid body is also considered. The temperature-dependent factor Φ is parameterized as Φ =exp$\{-aT^2/E_d\}$ following the work of Ignatyuk et al. (10). The shell dumping energy E_d is chosen to be 20 MeV. The intrinsic energy of the composite system E_{int} is calculated for each trajectory as

$$E_{int} = E^* - \frac{1}{2}\left(m^{-1}\right)_{ij} p_i p_j - V(q, l, T), \tag{4}$$

where E^* denotes the excitation energy of the compound nucleus, and is given by $E^* = E_{cm} - Q$ with Q and E_{cm} denoting the $Q-$value of the reaction and

the incident energy in the center-of-mass frame, respectively.

We take into account neutron emission in the Langevin calculation during the fusion-fission process. The present work is the first theoretical attempt to investigate neutron evaporation in the dynamical calculation of the fusion-fission process in the superheavy-mass region. Here, we assume that no neutron is emitted in the approaching process. Using the procedure outlined by Fröbrich et al. (11), in which the Langevin calculation and the statistical model were combined, the emission of neutrons has been coupled to the three-dimensional Langevin equation for the fusion-fission process. Due to the strong friction in this model, we assume that the kinetic energy of relative motion quickly dissipates into the intrinsic energy after contact. The thermal equilibrium in the composite system in this calculation is realized immediately within the time order of 10^{-22} s (12). We also assume that the particle emissions in the composite system are limited to neutron evaporation in the neutron-rich heavy nuclei.

The width of neutron emission is expressed as

$$\Gamma_n = g_n \frac{1}{2\pi\rho_A(E_{int})} \int_0^{E_{int}-B_n} \sum_l (2l+1) T_l(\epsilon) \rho_{A-1}(E_{int} - B_n - \epsilon) d\epsilon, \qquad (5)$$

where g_n is the spin multiplicity of the neutron. B_n and ϵ denote the neutron separation energy and the kinetic energy of the emitted neutron, respectively. The transmission coefficient is presented by T_l. The nuclear level density is denoted by $\rho(E)$ with suffixes A and $A-1$ for the compound nucleus and the residual one, respectively. R is the radius of the compound nucleus. Using the sharp cut off treatment for the angular momentum distribution of T_l, we express Eq. (5) as follow:

$$\Gamma_n = g_n \frac{1}{2\pi\rho_A(E_{int})} \frac{2\mu R^2}{\hbar^2} \int_0^{E_{int}-B_n} \epsilon \rho_{A-1}(E_{int} - B_n - \epsilon) d\epsilon. \qquad (6)$$

where μ is the neutron mass (13; 14). In the case of the excitation energy corresponding to a high incident energy compared with the Bass barrier height (15), as in the present case, the integration can be performed approximately, if we assume a simple form of $\rho(E) \propto e^{2\sqrt{a_n E}}$ for the level density (13), as follows:

$$\Gamma_n \simeq g_n \frac{\mu R^2}{\pi\hbar^2 a_n} (E_{int} - B_n) \exp\{-\sqrt{\frac{a_n}{E_{int}}} B_n\}, \qquad (7)$$

where a_n is the level density parameter.

The Langevin calculation is solved by using constant time steps Δt, and during each time step, the neutron emission is calculated by the following Monte Carlo procedure. We obtain the lifetime of neutron emission $\tau_n = \hbar/\Gamma_n$ from Eq.(7). The probability of neutron emission during the time interval Δt is described by $\frac{\Delta t}{\tau_n}$. If the ratio $\frac{\Delta t}{\tau_n}$ (in the actual calculation, $\Delta t < \tau_n$) is larger than a random number ξ ($0 \leq \xi \leq 1$), the emission of a neutron is registered. The kinetic energy of the emitted neutron $\epsilon^{(i)}$ is estimated stochastically by assuming the neutron spectrum from the composite system with the temperature T to be $\epsilon^{1/2} \exp(-\epsilon/T)$. The upper index (i) indicates the i-th neutron emission stage. Therefore, the energy loss in the neutron evaporation process is estimated as $-\epsilon^{(i)} - B_n^{(i)}$. Then we set a new intrinsic energy $E_{int}^{(i)} = E_{int}^{(i-1)} - \epsilon^{(i)} - B_n^{(i)}$, where for $i = 1$, $E_{int}^{(0)}$ means the initial value of E_{int}. The potential energy surface also changes as described by Eq.(2) as the temperature decreases. After the initial energy is reset, we proceed to the next time step of the Langevin calculation.

3 Results and discussion

Using our model, we analyze the experimental data in the reaction ^{58}Ni+^{208}Pb at E^*=185.9 MeV (3). Figure 1 shows the experimental result, which is the distribution of the pre-scission neutron multiplicity ν_n in correlation with fission fragments whose mass number is greater than $\frac{A}{2} - 30$ and less than $\frac{A}{2} + 30$.

An interesting feature of the distribution of pre-scission neutron multiplicity is its shape having two components, which are located around $\nu_n = 4$ and $\nu_n = 8$. This structure may be the sign of a simultaneous coexistence of two mechanisms corresponding to different life time of the composite system but to the phenomena giving nearly the same mass fragment in the fission process. The first one, defined as the QF process, would lead to the emission of about 4 neutrons only and for the second one, associated here with the FF process via a compound nucleus, would be found around 8 neutron emission. In this case, the fission process would tail long enough time to allow the emission of nearly 8 neutrons. By our model calculation, we try to confirm that the different dynamical processes, i.e., the FF process and the QF process, are giving different pre-scission neutron multiplicities in spite of the phenomenon associated with the similar mass fragment.

As mentioned in the previous section, in the calculation of neutron emission, there exist two important parameters, the level density parameter a_n and the neutron binding energy B_n. Both of these parameters depend on the deformation of the nucleus. In the dynamical calculation itself, another unknown factor is the dissipation energy E_{diss}, which is converted from the relative kinetic energy of the colliding system to the intrinsic energy during the approaching process. In this section, first we present the structure appeared in

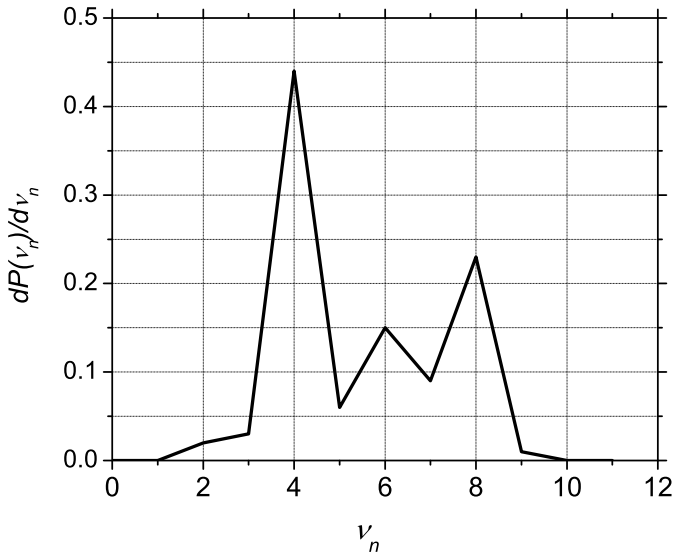

Fig. 1. Experimental pre-scission neutron multiplicity associated with fission fragment measurements in the reaction ^{58}Ni+^{208}Pb at E^*=185.9 MeV (3).

our model calculation of the pre-scission neutron multiplicity. Secondly, we discuss how the results depend on the parameters mentioned above.

3.1 Neutron emission during fusion-fission process

As discussed in reference (2), in order to simplify the calculation, we assume again that the kinetic energy does not dissipate during the approaching process, that is, $E_{diss} = 0$ MeV. In subsection 3.2.2 below, the sensitivity of E_{diss} is discussed. In the three-dimensional Langevin calculation, we prepare 1,000 trajectories, and at $t = 0$, each trajectory starts from the point of contact, which is defined as $R_{touch} = R_p + R_t$, where R_p and R_t are the radii of the projectile and the target, respectively.

The level density parameter a_n for a certain nuclear shape has been estimated by classical methods (16). Fundamentally, we need a_n for various deformations of the nucleus. According to reference (16), the value of a_n increases with increasing deformation of the nucleus. In order to simplify the calculation, we use two different values of a_n, that is, the value inside the fusion box defined in the deformation space as $\{z < 0.5, \delta < 0.3, |\alpha| < 0.3\}$, and that outside the region, which are denoted by a_n^{sph} and a_n^{def}, respectively. The excitation energy dependence of a_n is not considered. The neutron binding energy B_n also depends on the deformation, but here we use the constant value given for the ground state, because the fluctuation of B_n in the entire deformation

space relevant to the present calculation is ±0.3MeV. The influence of the fluctuation of B_n is discussed further in subsection 3.2.4. We chose the values of a_n^{sph} and a_n^{def} so as to reproduce the features of the experimental data, which are $a_n^{sph} = A/12.0$ and $a_n^{def} = A/10.0$.

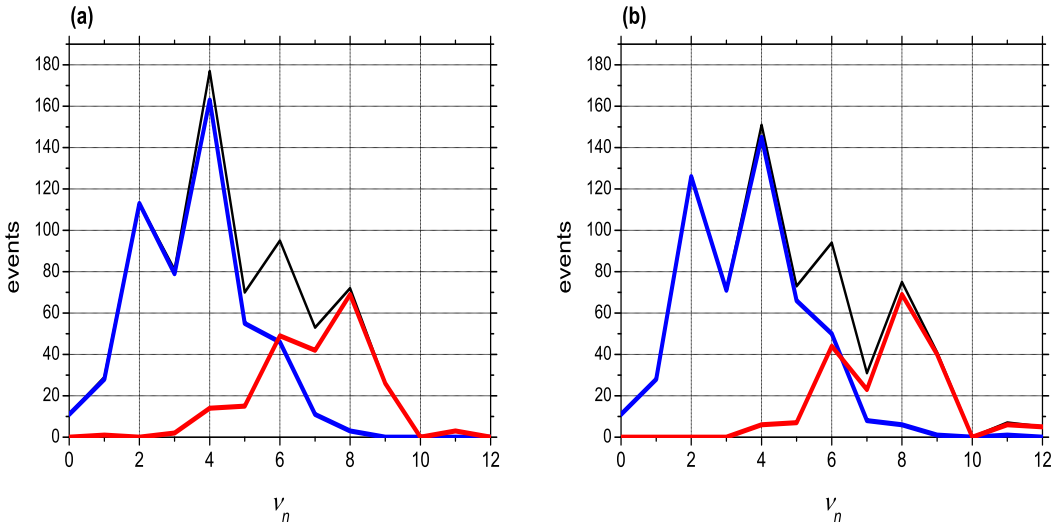

Fig. 2. Pre-scission neutron multiplicity given by our theoretical calculation in the reaction ^{58}Ni+^{208}Pb at E^*=185.9 MeV. The neutron multiplicity from the QF process and the FF process are denoted by the blue and red line, respectively. The black line denotes the total processes. (a) in the case of $a_n^{sph} = A/12.0$ and $a_n^{def} = A/10.0$ (b) in the case of $a_n^{sph} = A/14.0$ and $a_n^{def} = A/10.0$.

For the QF process, we plot the pre-scission neutron multiplicity in correlation with fission fragments with mass numbers greater than $\frac{A}{2} - 30$ and less than $\frac{A}{2} + 30$. To classify the trajectory of the FF path, the definition of the fusion area in the deformation space is very important. Here, we define the fusion area (fusion box) as the inside of the fission saddle point in the system described above. The idea behind the definition of the fusion box is the same as that in reference (2). The FF trajectory is identified as that which enters the fusion box.

The distribution of the pre-scission neutron multiplicity ν_n calculated by our model is shown in Fig. 2(a) with the level density parameters $a_n^{sph} = A/12.0$ and $a_n^{def} = A/10.0$. The pre-scission neutron multiplicity for the QF and the FF processes are denoted by the blue and the red lines, respectively. The black line shows the total multiplicity of each process. As another example, we show in Fig. 2(b) the result using the different level density parameter set, which are $a_n^{sph} = A/14.0$ and $a_n^{def} = A/10.0$.

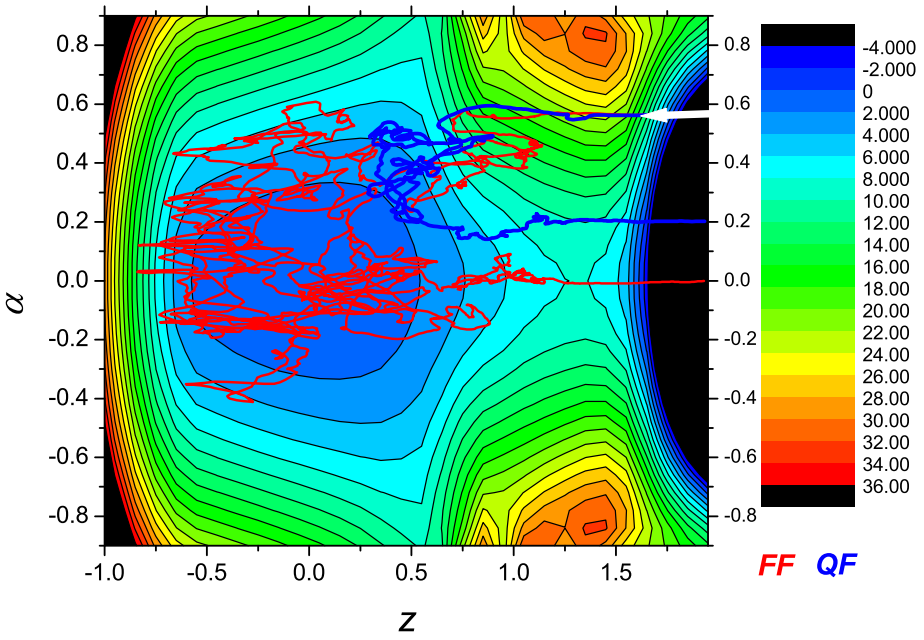

Fig. 3. Sample trajectories projected onto $z-\alpha$ ($\delta = 0$) plane at $E^* = 185.9$ MeV in the reaction ^{58}Ni+^{208}Pb. The trajectories of the QF and the FF processes are denoted by blue and red lines, respectively. The potential energy surface is presented by the liquid drop model in nuclear deformation space for ^{266}Ds. The arrow denotes the injection point of the reaction.

We can see clearly the two components which come from the QF process and the FF process. It is shown that for the large neutron multiplicity it originates from the FF path, and on the other hand for small neutron multiplicity it comes from the QF path. This means that the pre-scission neutron multiplicity has a strong correlation with dynamical paths.

On the pre-scission neutron multiplicity, the odd-even oscillations appear clearly, due to the odd-even effect on neutron binding energies. In the system, the initial number of neutrons is even, so that the probability of emitting an even number of neutrons is larger. The calculations show the similar structure observed in the experimental measurements in Fig. 1.

Next, we discuss the details on this calculation. Figures 3 and 4 show the potential energy surface of the liquid drop model for ^{266}Ds on the $z-\alpha$ ($\delta = 0$) plane and $z-\delta$ ($\alpha = 0$) plane, respectively, in the case of $l = 0$. This potential energy surface is calculated using the two-center shell model code (17; 18). The contour lines of the potential energy surface are drawn at steps of 2 MeV. Similar to the deformation parameters of nuclear shape described in reference (2), z is defined as $z = z_0/(R_{CN}B)$, where R_{CN} denotes the radius of the spherical compound nucleus. The parameter B is defined as

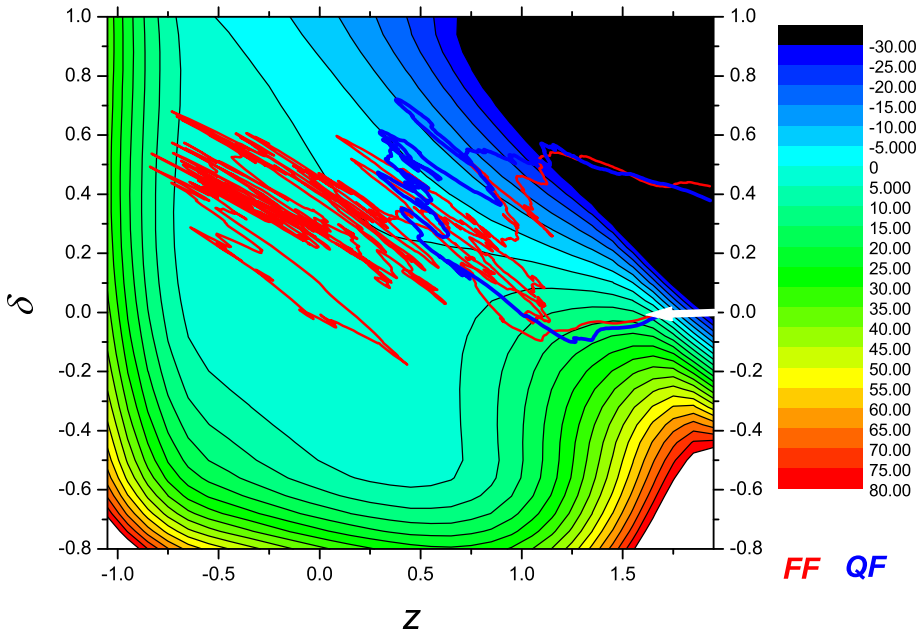

Fig. 4. The same samples of the trajectory as in Fig. 3, but which are projected onto $z - \delta$ ($\alpha = 0$) plane.

$B = (3 + \delta)/(3 - 2\delta)$.

In Figs. 3 and 4, the position at $z = \alpha = \delta = 0$ corresponds to a spherical compound nucleus. The injection point of this system is indicated by the arrow. The top of the arrow corresponds to the point of contact in the system. We start the calculation of the three-dimensional Langevin equation at the point of contact, which is located at $z = 1.575, \delta = 0.0, \alpha = 0.564$. All trajectories start at this point with momentum in the initial channel. That is to say, the initial velocity is directed in only the z direction, and the components of the initial velocities along the δ and α directions are both assumed to be zero. The sample trajectories of the QF process and the FF process are shown in Figs. 3 and 4. The trajectories are projected onto the $z - \alpha$ plane ($\delta = 0$) in Fig. 3 and $z - \delta$ plane ($\alpha = 0$) in Fig. 4. The trajectory of the QF process and the FF process are denoted by blue line and red line, respectively.

We define the travelling time t_{trav} as a time duration during which the trajectory moves from the point of contact to the scission point. Figure 5 shows the distribution of travelling time t_{trav}. The t_{trav} from the QF and FF processes are denoted by the solid and dashed lines, respectively. On the FF process, as we can see in Figs. 3 and 4, the trajectory is trapped in the pocket around the spherical region. The trajectory spends a relatively long time in the pocket and it has a large chance to emit neutrons. In average, the time duration spending

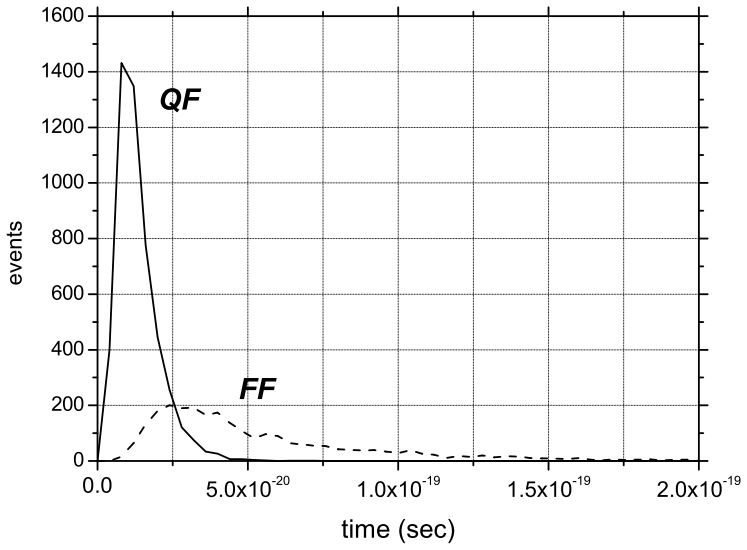

Fig. 5. The distribution of travelling time t_{trav} in the reaction ^{58}Ni+^{208}Pb at $E^* = 185.9$ MeV. The t_{trav} from the QF and FF processes are denoted by the solid and dashed lines, respectively.

in the pocket is 7×10^{-20}sec. On the other hand, the trajectory of the QF process reaches to the scission point quickly. So, it has not so much chance to emit neutrons. The mean travelling time for the QF process is approximately 2×10^{-20}sec.

Actually the distribution of t_{trav} for each trajectory is clearly distinguished by the two processes as shown in Fig. 5. The time scale of the FF process is about 3 or 4 times longer than that of the QF process. We can see in Figs. 3 and 4 that the length of QF path is shorter than that of the FF path. On the other hand, the FF trajectory is trapped at the potential pocket near spherical region, so that the traveling time becomes longer.

It is interesting to investigate the correlation between the travelling time and a number of events for neutron multiplicity. Figure 6 shows the relation of the travelling time t_{trav} and pre-scission neutron multiplicity ν_n. The blue dots and red dots are denoted the events for the QF and the FF processes, respectively. As shown in Fig. 6, the longer the travelling time is, the larger the pre-scission neutron multiplicity becomes. Also in the figure, the correlation between the mass distribution of fission fragments and the pre-scission neutron multiplicity is shown. The events from the QF process are distributing around $\nu_n = 2n, 3n$ and $4n$, and in the time axis they are distributing around $t_{trav} \sim 1.5 \times 10^{-20}$ sec. In the case of the FF process, due to longer t_{trav}, the events are scattered around $\nu_n = 6n, 7n$ and $8n$. Since the mass distribution of fission fragments shows symmetric in this reaction system due to high incident energy, we can

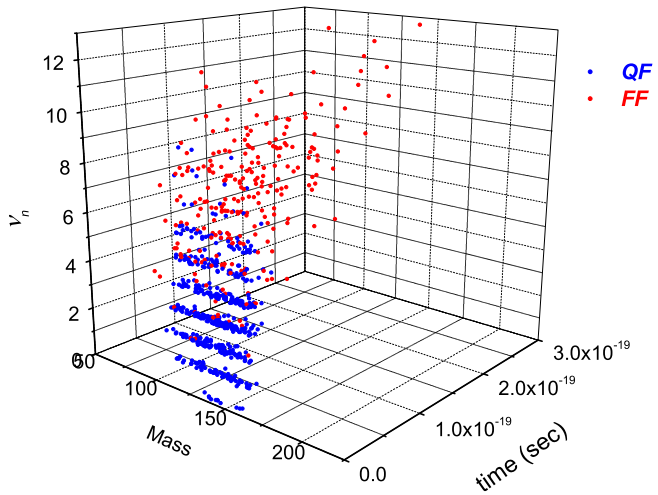

Fig. 6. The relation of the travelling time t_{trav}, the mass distribution of fission fragments and pre-scission neutron multiplicity ν_n. The blue and red dots are denoted the events from the QF and FF processes, respectively.

not clearly see the correlation between the mass fragment and the neutron multiplicity.

3.2 Parameter dependence of the model

Our model has several parameters which are not confirmed theoretically at present. We discuss the sensitivity of the parameters of our model and show clearly the role of each parameter. As the essential factors that influence the neutron multiplicity, two categories are considered. They are concerned with the travelling time of the trajectory and with the rate of neutron emission. The former comprises the strength of the friction force and the dissipation energy E_{diss} at the point of contact. The latter comprises the level density parameter a_n and the neutron binding energy B_n.

3.2.1 Friction force γ

In the dynamical calculation, the friction force plays a very important role. The friction force influences mainly the travelling time of the trajectory. Moreover, the rate of dissipation at which the relative kinetic energy is converted into the intrinsic energy and the strength of fluctuation in the trajectory are controlled by the magnitude of the friction force. In order to elucidate the sensitivity of the one-body friction tensor to the trajectory calculation, the pre-scission

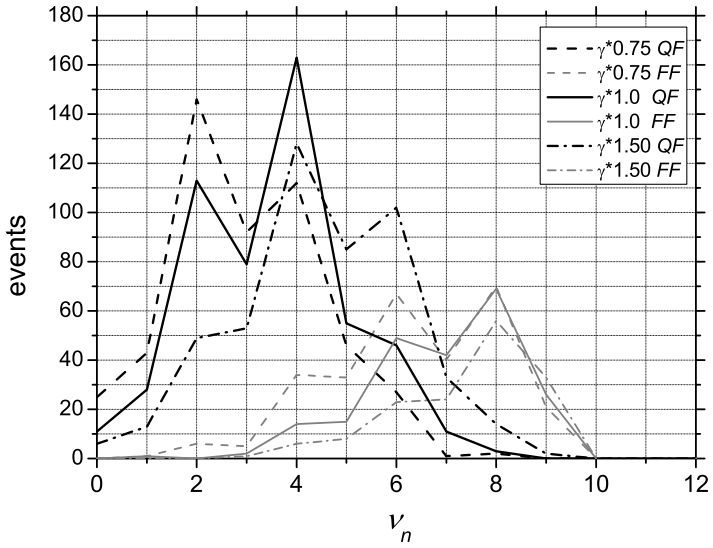

Fig. 7. The neutron multiplicity calculated using one-body friction tensor multiplied by factors 0.75, 1.0 and 1.5, as denoted by the dashed, solid and dashed-dotted lines, respectively. The neutron multiplicity of the QF and FF processes is dented by the black and gray lines, respectively.

neutron multiplicity is shown in Fig. 7 for the modified strength of the one-body friction tensor. The multiplied factors are 0.75, 1.0 and 1.5, and the corresponding results are shown by the dashed, solid and dashed-dotted lines, respectively. The neutron multiplicities from the QF and FF processes are dented by the black and gray lines, respectively.

For large friction with the factor of 1.5, the trajectory speed is slower than that in the case of friction with the factor of 1.0. Due to longer t_{trav}, the neutron multiplicity ν_n becomes larger. As a result, the peaks of neutron multiplicity from the QF process and the FF process shift to larger multiplicity (to the right in Fig. 7). On the other hand, in the case of the factor of 0.75 (smaller friction), the trajectory speed is faster and the neutron multiplicity distribution shifts to smaller ν_n.

3.2.2 Dissipation energy E_{diss}

As the initial condition of the Langevin calculation, the intrinsic energy and relative kinetic energy of nuclei at the point of contact are very important. However, in the superheavy-mass region, it is an open question as to how much of the relative kinetic energy of the colliding system dissipates into intrinsic energy during the approaching process. Although we assume no energy dissipation E_{diss} at the point of contact in our model calculation, in order to

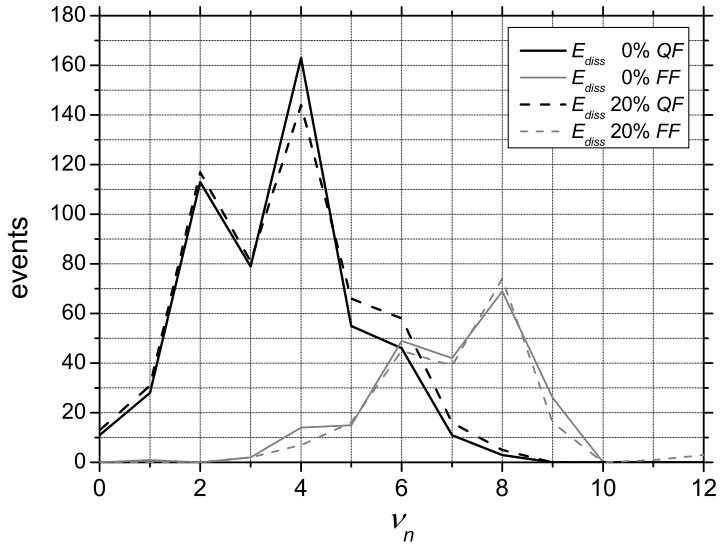

Fig. 8. The neutron multiplicity in the cases of $E_{diss} = 0$ and 32.4 MeV, as denoted by solid and dashed lines, respectively. The black and gray lines denote the neutron multiplicity from the QF and FF processes, respectively.

elucidate the sensitivity of E_{diss}, we deal with it at that point as a parameter. We have discussed this subject on the basis of an analysis of the mass distribution of fission fragments in reference (19). Here, we discuss how the energy loss E_{diss} affects the neutron multiplicity.

Since the initial momentum in the $-z$ direction strongly affects the trajectory, E_{diss} is expected to play a substantial role. Figure 8 shows the neutron multiplicity in the cases of $E_{diss} = 0$ and 32.4 MeV (20% of kinetic energy dissipates), which are denoted by solid and dashed lines, respectively. The black and gray lines denote the neutron multiplicity from the QF and FF processes, respectively.

In the case of E_{diss}=32.4 MeV, due to the smaller initial momentum in the $-z$ direction, the number of trajectories that reach the spherical area decreases. However, due to the odd-even effect on the neutron binding energies, such a variance of initial momentum is too small to significantly change the neutron multiplicity distribution.

Quantitatively, the mean value of ν_n for the QF process increases from 3.53 to 3.60 when 20% of the kinetic energy is converted to the internal one during the approaching process. On the contrary, in the same situation, the mean value of ν_n for the FF process decreases from 7.94 to 7.87.

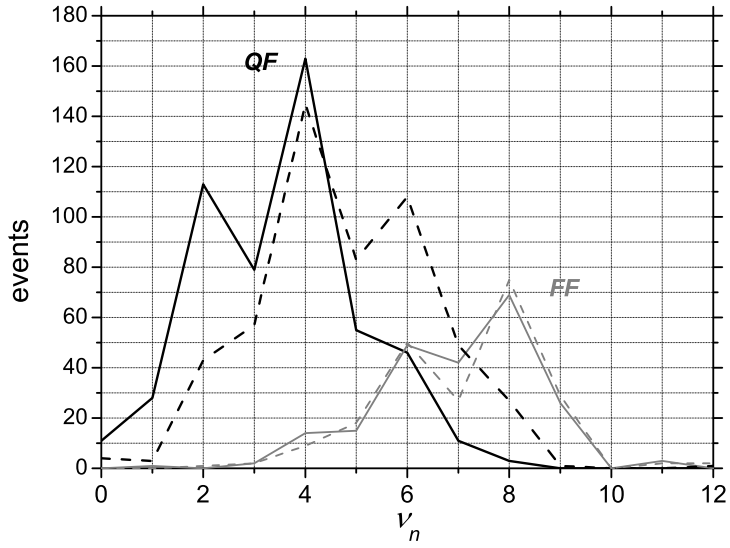

Fig. 9. The neutron multiplicity calculated using $a_n = A/12.0$ in the entire deformation space, denoted by the dashed lines. The solid lines denote the calculation using $a_n^{sph} = A/12.0$ and $a_n^{def} = A/10.0$. The black and gray lines denote the QF and FF processes, respectively.

3.2.3 Level density parameter a_n

In the statistical model calculation, the level density parameter a_n is very important. The lifetime of neutron emission is strongly affected by a_n, because a_n appears in the exponent in the formula of the decay width, as shown by Eq. (7).

First, we use the constant value a_n in the entire deformation space. The value of a_n is chosen so as to reproduce the experimental data of the neutron multiplicity from the spherical region, that is, to reproduce the peak which is located at ν_n=8, where $a_n = A/12.0$ is used. The neutron multiplicity in this case is shown by the dashed lines in Fig. 9. The black and gray lines denote the neutron multiplicity from the QF and FF processes, respectively. We can see that the value at $\nu_n = 6$ is rather large, which is not consistent with the present experimental data.

According to reference (16), a_n depends on the deformation. As we did in the previous section, we use a different value inside the fusion box and outside of it, $a_n^{sph} = A/12.0$ and $a_n^{def} = A/10.0$, respectively. We also plot this result in Fig. 9 as the solid lines. Due to the larger value of a_n^{def} in the deformation space compared with a_n^{sph}, the emission rate of neutrons on the QF path decreases.

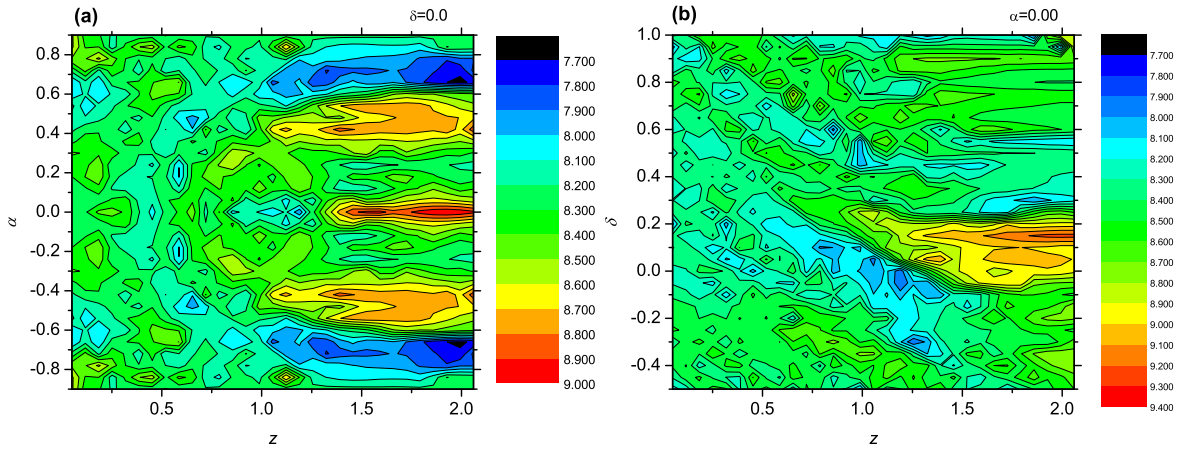

Fig. 10. The neutron binding energy B_n of ^{266}Ds on the deformation space. (a) $z-\alpha$ ($\delta = 0$) plane. (b) $z-\delta$ ($\alpha = 0$) plane.

3.2.4 Neutron binding energy B_n

Another parameter that strongly influences the decay width for neutron emission is the neutron binding energy, B_n, of the composite system. As shown in Eq. (7), B_n influences the lifetime of neutron emission in the same manner as does a_n. B_n depends on the deformation of the nucleus. Figure 10(a) and (b) shows B_n of ^{266}Ds on the $z-\alpha$ ($\delta = 0$) plane and $z-\delta$ ($\alpha = 0$) plane, respectively. Here, we use the two-center shell model code (17; 18). We can see that in the whole deformation space, the neutron binding energy fluctuates by about ± 0.3 MeV comparing with that for spherical compound nucleus.

We investigate the B_n dependence of the neutron multiplicity. In the same way as in the case of a_n, we use a different value of B_n inside the fusion box (B_n^{sph}) and outside of it (B_n^{def}). B_n^{sph} means the neutron binding energy of the compound nucleus. Figure 11 shows the neutron multiplicity for three different sets of B_n^{def}, that is to say, $B_n^{def} = B_n^{sph}$, $B_n^{def} = B_n^{sph} - 0.3$ and $B_n^{def} = B_n^{sph} + 0.3$, as denoted by the solid, dashed and dashed-dotted lines, respectively. The black and gray lines denote the QF and FF processes, respectively. The larger value of B_n causes the emission rate of neutrons to decrease. As a result, the distribution of the neutron multiplicity shifts to smaller multiplicity (to the left in Fig. 11). The large value of B_n contributes the neutron multiplicity in the same manner as the large value of a_n.

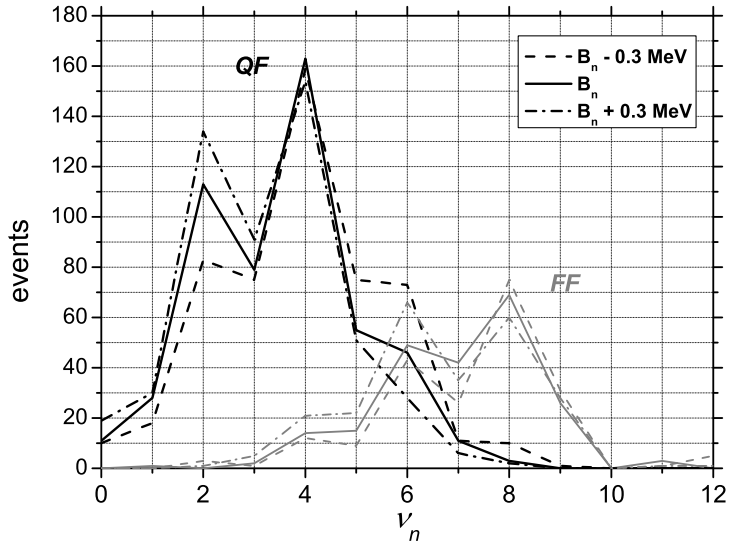

Fig. 11. The neutron multiplicity calculated using $B_n^{def} = B_n^{sph}, B_n^{sph} - 0.3$, and $B_n^{sph} + 0.3$, as denoted by the solid, dashed and dashed-dotted lines, respectively. B_n^{sph} means the neutron binding energy of the compound nucleus. The black and gray lines denote the QF and FF processes, respectively.

4 Summary

We introduced the effect of pre-scission neutron emission into the three-dimensional Langevin calculation, that is to say, we combined the Langevin code with the statistical code. We applied our model to the investigation of the whole fusion-fission dynamical path in the reactions ^{58}Ni+^{208}Pb at E^*=185.9 MeV (3).

Our model is successfully applied to distinguish between the FF process and the QF process in terms of the pre-scission neutron multiplicity. We can see clearly the two components of the neutron multiplicity, which come from the QF process and the FF process. It is found that the peak for the large neutron multiplicity originates from the FF path, and on the other hand the peak for small neutron multiplicity comes from the QF path. The pre-scission neutron multiplicity has a strong correlation with dynamical path and is a powerful tool for investigating fusion-fission mechanism.

We also discussed the sensitivity of the parameters of our model and showed clearly the role of each parameter. As the essential factors that influence the neutron multiplicity, we investigated the friction force γ, dissipation energy E_{diss}, level density parameter a_n and neutron binding energy B_n.

This study will be the cornerstone for further study which develops the methods of the classification between the FF process and the DQF process. The

DéMoN group already has measured the pre-scission neutron multiplicity in reactions, ^{48}Ca+^{208}Pb, ^{48}Ca+^{244}Pu and ^{58}Fe+^{248}Cm at $E^* \sim 40$ MeV (20; 21). In the next study, we would like to analyze these reactions.

The authors are grateful to Professor Yu. Ts. Oganessian, Professor M.G. Itkis, Professor V.I. Zagrebaev for their helpful suggestions and valuable discussion throughout the present work. The authors thank Dr. S. Yamaji and his collaborators, who developed the calculation code for potential energy with a two-center parameterization. This work has been in part supported by INTAS projects 03-01-6417.

References

[1] M.G. Itkis et al., Proc. of Fusion Dynamics at the Extremes (World Scientific, Singapore, 2001) p93.
[2] Y. Aritomo and M. Ohta, Nucl. Phys. A**744** (2004) 3.
[3] L. Donadiile et al, Nucl. Phys. A **656** (1999) 259.
[4] J. Maruhn and W. Greiner, Z. Phys. **251** (1972) 431.
[5] K. Sato, A. Iwamoto, K. Harada, S. Yamaji, and S. Yoshida, Z. Phys. A **288** (1978) 383.
[6] J. Blocki, Y. Boneh, J.R. Nix, J. Randrup, M. Robel, A.J. Sierk and W.J. Swiatecki, Ann. Phys. **113** (1978) 330.
[7] J.R. Nix and A.J. Sierk, Nucl. Phys. A **428** (1984) 161c.
[8] H. Feldmeier, Rep. Prog. Phys. **50** (1987) 915.
[9] H.J. Krappe, J.R. Nix, and A.J. Sierk, Phys. Rev. **C20** (1979) 992.
[10] A.V. Ignatyuk, G.N. Smirenkin, and A.S. Tishin, Sov. J. Nucl. Phys. **21** (1975) 255.
[11] P. Fröbrich, I.I. Gontchar and N.D. Mavlitov, Nucl Phys, A **556** (1993) 281.
[12] Y. Aritomo, Ph. D. Thesis, Konan university, Kobe 1998.
[13] R. Vandenbosch and J.R. Huizenger, *Nuclear Fission* (Academic Press, New York, 1973), p.233.
[14] M. Ohta, Proceeding of *Fusion Dynamics at the Extremes*, Dubna, May 25 -27, 2000 (World Scientific, Singapore, 2001) p.110.
[15] R. Bass, Nucl. Phys. **A231** (1974) 45.
[16] J. Toke and W.J. Swiatecki, Nucl. Phys. A**372** (1981) 141.
[17] S. Suekane, A. Iwamoto, S. Yamaji and K. Harada, JAERI-memo, (1974) 5918.
[18] A. Iwamoto, S. Yamaji, S. Suekane and K. Harada, Prog. Theor. Phys. **55** (1976) 115.
[19] Y. Aritomo and M. Ohta, Yderna Fiz. **66** (2003) 1141.
[20] T. Materna et al., Nucl. Phys. **A734** (2004) 184; T. Materna et al., Prog.

Theo. Phys. No. 154 (2004) 442; T. Materna et al., Int. Jour. Mod. Phys. E.**13** (2004) 258.
[21] N. Amar, Ph. D. Thesis, Universite de Caen, Basse-Normandie 2003.